JOURNAL OF GUIDANCE, CONTROL, AND DYNAMICS
Vol. 29, No. 1, January–February 2006

Phase Space Structure Around Oblate Planetary Satellites

Juan F. San-Juan*
Universidad de La Rioja, 26004 La Rioja, Spain
Martín Lara†
Real Observatorio de la Armada, 11110 Cádiz, Spain
and
Sebastián Ferrer‡
Universidad de Murcia, 30071 Murcia, Spain

The dynamics of an orbiter around planetary satellites are modeled using Hill's equations perturbed by the nonsphericity of the satellite. Classically, the long-term behavior of this problem is studied by averaging techniques. The double-averaged problem is integrable. However, up to second order, it presents a symmetry of direct and retrograde inclination orbits that do not exist in the original problem. Lie transforms are used to reduce the problem to an integrable one, with the transformations performed up to third order where the inclination symmetry is broken. Then, by the use of the double reduced space, which is a sphere, a full description of families of frozen orbits and their bifurcations is given. Saddle-center and pitchfork bifurcations related to stable, frozen orbits are identified. Finally, for the specific case of a Europa orbiter, the equilibria of the reduced problem are related to periodic solutions of the nonaveraged problem in a synodic frame.

Nomenclature

a = semimajor axis (orbital element)
e = eccentricity (orbital element)
f = true anomaly
G = modulus of angular momentum vector (Delaunay variable)
g = argument of perigee (Delaunay variable)
H = projection of angular momentum vector on symmetry axis (Delaunay variable)
$\mathcal{H}$ = Hamiltonian function
h = argument of node in rotating frame (Delaunay-type variable), $\Omega - l'$
i = inclination (orbital element)
J_2 = satellite's nonspherical coefficient
$\mathcal{K}$ = Hamiltonian of Lidov–Kozai model
L = conjugate momentum to mean anomaly (Delaunay variable)
l = mean anomaly (Delaunay variable)
l' = mean anomaly of perturbing body
n = mean motion of orbiter
P_2 = Legendre polynomial of degree 2
p = semilatus rectum
r = distance from orbiter to origin
u = argument of latitude, $f + g$
W = effective potential
$\boldsymbol{X}$ = (X, Y, Z) conjugated momenta to $\boldsymbol{x}$
$\boldsymbol{x}$ = (x, y, z) position vector of orbiter
α = equatorial radius of satellite
β = ratio between J_2 and third-body perturbations
δ = auxiliary function; defined in Eq. (15)
ϵ = fictitious small parameter
η = eccentricity function
μ = gravitational parameter: gravitational constant times mass of body
ξ_j = coordinates in sphere, $j = 1, 2, 3$
Ω = argument of node (orbital element)
ω = angular velocity of rotating frame

Presented as Paper 2004-4863 at the AIAA–AAS Astrodynamics Specialist Conference, Providence, RI, 16–19 August 2004; received 13 September 2004; revision received 8 February 2005; accepted for publication 9 February 2005.

*Associate Professor, Departamento de Matemáticas y Computación, Logroño; juanfelix.sanjuan@dmc.unirioja.es.
†Commander, Department Ephemerides, San Fernando; mlara@roa.es. Member AIAA.
‡Professor, Departamento de Matemática Aplicada; sferrer@um.es.

Introduction

THE proposed Jupiter Icy Moons Orbiter mission[1] to the Galilean satellites motivates renewed interest in the study of orbital dynamics around planetary satellites. The main features of the dynamics close to the planetary satellite are described using Hill's model.[2] A more realistic model was proposed by Kozai,[3] in application to the motion of a satellite of the moon, that also accounts for the perturbation of the satellite's nonsphericity. Lidov[4] used this approach to demonstrate the stability of the orbits of the satellites of Uranus.

Lidov and Yarskaya[5] use Hill's approximation for modeling the perturbing acceleration due to the third body and take the nonsphericity of the central body into account by retaining its second zonal harmonic. Under the assumption that there are not resonant relations between the frequencies of the satellite and the third body's rotations, the Lagrange planetary equations lead to seven cases where the double-averaged problem is integrable. Of particular interest is Lidov's case 3, where the equatorial plane of the planet coincides with the orbital plane of the perturbing body. This case was recently used by Scheeres et al.[6] for analyzing the stability of almost-circular orbits around the Jovian moon Europa.

In this work, we use the Lidov–Kozai model for describing the phase space around planetary satellites. We use a Hamiltonian formulation and resort to general perturbation methods to provide an analytical theory for the motion of an orbiter around a planetary satellite, especially for the dynamics of the perigee. However, we do not constrain ourselves to a simple first-order averaging, and we provide a full description of the phase space averaged to a higher order.

We reduce the problem to two degrees of freedom by the classical Delaunay normalization (see Ref. 7) that averages the problem over the mean anomaly. A further reduction is performed to remove the argument of the node. After the nonsymmetry is manifest, truncation and reduction lead us to an integrable differential system in the variables g and G that depends on H and L, which, in the reduced

system, are dynamic parameters. Note that all of the transformations are developed in closed form of the eccentricity, and, therefore, our theory is not limited to almost-circular orbits.

The qualitative behavior of the problem for each value L and H on the parametric plane can be described without the need to integrate the reduced differential system. Bifurcation lines on the (L, H) plane are defined by changes in the number of equilibrium solutions, or frozen orbits. These lines are obtained as solutions of the nonlinear algebraic system $\dot{g} = 0$, $\dot{G} = 0$, by classical polynomial algebra. In each region defined by the bifurcations lines, phase portraits can be "painted"[8,9] for different values of the parameters.

Finally, for the particular case of an orbiter around Europa, we relate the equilibria of the double-averaged problem to periodic synodic solutions of the nonaveraged problem previously identified and studied in Ref. 10, which we believe supports the validity of our analytic theory. Of course, the validity of our theory is restricted to a region in phase space close enough to the central body, where we assume that Hill's assumptions apply.

Dynamic Model

We consider the motion of an orbiter around a natural satellite of a planet. The mass of the orbiter is taken to be so small that it does not influence the motion of both the planet and the satellite, which are assumed to be in circular orbits about their mutual center of mass. We further assume that the distance between the centers of mass of the planet and the satellite is long enough to consider the planet as a mass point and that the equator of the satellite coincides with its orbital plane.

When Hamiltonian formulation is used in the planet-fixed rotating frame, the problem can be written as

$$\mathcal{H} = \tfrac{1}{2}(\boldsymbol{X}\cdot\boldsymbol{X}) - \omega\cdot(\boldsymbol{x}\times\boldsymbol{X}) + W(\boldsymbol{x}) \tag{1}$$

and when the planetary perturbation in Hill's approximation and the oblateness of the satellite are considered, the effective potential is

$$W = \tfrac{1}{2}\omega^2(r^2 - 3x^2) - (\mu/r)\left[1 - J_2(\alpha/r)^2 P_2(z/r)\right] \tag{2}$$

Note that a more general Hill perturbed (planar) model has been recently studied[11,12] where the oblateness of the perturbing body is of relevance. In our case, this is a higher-order effect, and we safely neglect it. However, because the Cartesian-synodic approach of Refs. 11 and 12 requires no averaging, it captures the short-periodic behavior in addition to the secular and long-periodic terms. Although this approach captures the complete rich dynamic behavior in the vicinity of an oblate satellite, it lacks the physical insight usually available only through analytical theories.

Details on the formulation of our dynamic model are given in Ref. 10. In this work we resort to perturbation theory to find a higher-order analytical solution of Eqs. (1) and (2). Our theory describes the nature of solutions and explains their dependence on physical and dynamic parameters. However, the short-period dynamics are lost in the process of averaging. In Ref. 10, not only the equations of motion for a large family of initial conditions were numerically integrated, but so were the variational equations. In addition, the results were not limited, to a planar problem, and results were presented for the three-dimensional case. This is of relevance to real missions. A well-known effect of the third-body perturbation is the change in the stability of circular orbits related to orbit inclination. The results in Ref. 10 are used later in this paper to test our third-order averaging.

The Hamiltonian Eq. (1) is made of the Keplerian attraction $\mathcal{H}_K$, the Coriolis term $\mathcal{H}_\omega$, the third-body perturbation $\mathcal{H}_{3b}$, and the oblateness perturbation $\mathcal{H}_{J_2}$

$$\mathcal{H} = \mathcal{H}_K + \mathcal{H}_\omega + \mathcal{H}_{3b} + \mathcal{H}_{J_2} \tag{3}$$

where, in classical orbital elements a, e, i, g, and Ω,

$$\mathcal{H}_K = -\tfrac{1}{2}(\mu/a)$$

$$\mathcal{H}_\omega = -(\mu/a)(\omega/n)\sqrt{1-e^2}\cos i$$

$$\mathcal{H}_{3b} = \tfrac{1}{2}(\mu/a)(\omega/n)^2(r/a)^2[1 - 3(\cos h\cos u - \cos i\sin h\sin u)^2]$$

$$\mathcal{H}_{J_2} = (\mu/a)J_2\,(a/r)(\alpha/r)^2 P_2(\sin i\ \sin u) \tag{4}$$

Lidov–Kozai Model to Third Order

Lidov and Yarskaya[5] use Lagrange planetary equations to investigate the secular evolution of the orbital elements of a satellite. They average the perturbing function over the mean anomalies of the satellite and the perturbing body and study the behavior of solutions of the secular equations, finding seven integrable cases. Of particular interest is their case 3 that was previously used by Kozai[3] from the point of view of perturbation theory.

Kozai assumes that the short-periodic terms have little effect on the satellite's motion and starts from a Hamiltonian where all terms in the mean longitude of the satellite are dropped. Furthermore, he assumes that the third-body and the oblateness perturbations are of the same order and performs canonical transformations to eliminate the argument of the node in the rotating frame. After the first-order transformation, Kozai finds an integrable system that is exactly the same as Lidov and Yarskaya's case 3. Therefore, we denote the Lidov–Kozai model as a model where the influence of the noncentrality of the planetary field and the third-body perturbation are considered to be of the same order.

However, the Lidov–Kozai model averaged to first order misses an important characteristic in the motion of an orbiter around a planetary satellite: the nonsymmetric behavior of direct and retrograde inclination orbits due to the cosine of the inclination present in $\mathcal{H}_{3b}$ and clearly noted in Refs. 6 and 10. We provide a qualitative analysis that reflects this characteristic and extend the canonical transformations to a higher order.

Reduction by Normalizations

We assume that the main influence is due to Keplerian attraction and that $J_2 \sim \mathcal{O}(\omega/n)^2$. Then, using Eq. (4), we can write Eq. (3) as a power series of ϵ

$$\mathcal{H} = \sum_{i=0}^{2}\left(\frac{\epsilon^i}{i!}\right)\mathcal{H}_i \tag{5}$$

where $\mathcal{H}_0 = \mathcal{H}_K$ and

$$\mathcal{H}_1 = (1/\epsilon)\mathcal{H}_\omega, \qquad \mathcal{H}_2 = (2/\epsilon^2)\left(\mathcal{H}_{J_2} + \mathcal{H}_{3b}\right) \tag{6}$$

The fictitious parameter ϵ is of the order of ω/n, and, following the example of previous works,[13,14] we take some bound of $|\mathcal{H}_\omega/\mathcal{H}_K|$ as the value of ϵ.

With the Hamiltonian written as a power series of ϵ, we can apply perturbation methods based on Lie transforms. More precisely, we implement two Lie transforms using Deprit's method.[15]

To apply perturbation theory, we found it convenient to use canonical (similar to) Delaunay variables l, g, h, L, G, and H, where the conjugated momentums are defined by

$$L = \sqrt{\mu\, a}, \qquad G = L\sqrt{1-e^2}, \qquad H = G\cos i \tag{7}$$

For convenience, we drop primes in those variables coming from the Lie transform processes.

Short-Period Elimination

Following the application made in Ref. 16 to the zonal problem of the artificial satellite problem, we first reduce the problem to two degrees of freedom by the classical Delaunay normalization (see Ref. 7). This transformation averages the problem over the mean anomaly for each order of perturbation, and the short period terms are removed from Eq. (5). Up to third order, we obtain

$$\mathcal{H}' = \sum_{i=0}^{3}\left(\frac{\epsilon^i}{i!}\right)\mathcal{H}'_i \tag{8}$$

where

$$\mathcal{H}'_0 = -\mu^2/(2L^2)$$

$$\mathcal{H}'_1 = -\tilde{\omega}H$$

$$\mathcal{H}'_2 = (1/4)\tilde{J}_2\mu(\alpha^2/p^3)(3s^2-2)\eta^3 + (1/8)a^2\tilde{\omega}^2(3\eta^2-5) \times [2-3s^2(1-\cos 2h)] + (15/16)a^2\tilde{\omega}^2(\eta^2-1)[(c-1)^2 \times \cos 2(g-h) + (c+1)^2\cos 2(g+h) + 2s^2\cos 2g]$$

$$\mathcal{H}'_3 = (45/16)a^2\tilde{\omega}^2(\tilde{\omega}/n)\eta(\eta^2-1)[(c+1)^2\cos 2(g+h) - (c-1)^2\cos 2(g-h)] \quad (9)$$

with $\eta = G/L$ and $p = G^2/\mu$ and where we introduced new constants

$$\tilde{\omega} = (1/\epsilon)\,\omega, \qquad \tilde{J}_2 = (2/\epsilon^2)J_2 \quad (10)$$

and c and s are abbreviations for cosine and sine of inclination. Note that all of the transformations are developed in closed form of the eccentricity.

Elimination of Node

A further reduction is performed to remove the argument of the node. Then, the reduced Hamiltonian depends only on the argument of the perigee. The scheme we follow was applied to the motion of a lunar orbiter,[3] the stellar three-body problem,[17] low artificial satellite problems,[18,19] and in a tesseral artificial satellite problem.[13,14,20] Explicit expressions up to third order of the new Hamiltonian are

$$\mathcal{H}'' = \sum_{i=0}^{3}\left(\frac{\epsilon^i}{i!}\right)\mathcal{H}''_i \quad (11)$$

where $\mathcal{H}''_0 = \mathcal{H}'_0$, $\mathcal{H}''_1 = \mathcal{H}'_1$, and

$$\mathcal{H}''_2 = \left[\tfrac{1}{8}(\tilde{\omega}/\mu)^2L^2G^2\right]\{(1-3H^2/G^2)[5L^2/G^2 + 4\beta/(G^5L^5) - 3] + 15\,(1-H^2/G^2)\,(1-L^2/G^2)\cos 2g\}$$

$$\mathcal{H}''_3 = \left[\tfrac{1}{8}(\tilde{\omega}/\mu)^2L^2G^2\right][(27/8)(\tilde{\omega}/\mu)^2L^2H/\tilde{\omega}] \times [33 + 17H^2/G^2 - 35L^2/G^2 - 15H^2L^2/G^4 + 15(1-H^2/G^2)\,(1-L^2/G^2)\cos 2g] \quad (12)$$

The parameter β is defined by the ratio between the J_2 and third-body perturbations:

$$\beta = \tfrac{1}{2}\tilde{J}_2(\alpha\mu^3/\tilde{\omega})^2 = J_2\,(\alpha\,\mu^3/\omega)^2 \quad (13)$$

This β is equivalent to other parameters used in the classical literature, except for a coefficient related to the semimajor axis a that is not present here.

In geometric terms, the two Lie transformations result in a toral reduction. In other words, after truncation, we have two integrals L and H corresponding to the ignorable variables. As soon as the system is integrated in g and G, we obtain ℓ and h by two quadratures.

Therefore, we obtained an integrable one-degree-of-freedom (DOF) problem in the variables g and G. To study this, we neglect the terms $\mathcal{H}_0$ and $\mathcal{H}_1$ from Eq. (11). After recovering the initial constants ω, and J_2, we obtain

$$\mathcal{K} = \tfrac{1}{16}(\omega/\mu)^2L^4 \times \{-15e^2s^2\cos 2g + (3s^2-2)[2+3e^2+4\beta/(G^3L^7)] - \delta[2s^2 + (50-17s^2+15s^2\cos 2g)e^2]\} \quad (14)$$

where $e^2 = 1 - G^2/L^2$, $s^2 = 1 - H^2/G^2$, and we introduced the function $\delta(L, H)$ given by

$$\delta = \tfrac{9}{8}(\omega/\mu^2)L^2H \quad (15)$$

Note that $|\delta(L, H)| < \epsilon$ because $\epsilon = 2|(\omega/\mu^2)H^*|L^{*2}$, where L^* and H^* are bounds for L and H.

The problem really depends on two dynamic parameters, H and L, and on two physical parameters, β and ω/μ^2. The latter are fixed for each orbiter; the former will change within the constraints of the model. The focus is usually put on the J_2 variation, and this explains why the semimajor axis appears as a fixed quantity in Lidov and Yarskaya's[5] parameter β, later used as ε by Scheeres et al.[6]

The system defined by Eq. (14) is what we call the third-order Lidov–Kozai model.

Differential System of Model

From the earlier Hamiltonian Eq. (14), we obtain the differential equations of the third-order Lidov–Kozai model: $\dot{g} = \partial\mathcal{K}/\partial G$ and $\dot{G} = -\partial\mathcal{K}/\partial g$:

$$\dot{g} = (3/8)(\omega/\mu)^2(L^4/G) \times \{-12 + 2(4-5s^2)\,\beta/(G^3L^7) + (1+\delta)[16\eta^2 - 5(\eta^2-c^2)\,(1-\cos 2g)]\} \quad (16)$$

$$\dot{G} = -(15/8)(\omega/\mu)^2L^4s^2(1-\eta^2)(1+\delta)\sin 2g \quad (17)$$

Equations (16) and (17) correspond to a one-DOF system. For a fixed value $\mathcal{K} = k_0$ of energy, we can solve Eq. (14) for $\cos 2g$. Then, $\sin 2g$ is a function of G and the parameters and Eq. (17) reduce to a quadrature:

$$t - t_0 = \int F\left(G; L, H, \beta, \frac{\omega}{\mu^2}, k_0\right)\mathrm{d}G \quad (18)$$

that uses a hyperelliptic integral. We are not interested in resolving the quadrature. We present only a qualitative analysis of the flow, as a function of the parameters involved. This sets up the specific initial conditions. Specific solutions of the quadrature Eq. (18) can be found in the literature.[6]

Europa Model

In the preceding study we considered both the oblateness and third-body perturbations to be of the same order. However, we must be more careful in investigating the relative influence of each perturbation when interested in a specific case. Thus, assuming that the principal influence is due to Keplerian attraction, we write Eq. (3) as

$$\mathcal{H} = \mathcal{H}_K[1 + (\mathcal{H}_\omega/\mathcal{H}_K) + (\mathcal{H}_{3b}/\mathcal{H}_K) + (\mathcal{H}_{J_2}/\mathcal{H}_K)] \quad (19)$$

Calling $\mathcal{H}^K_x = |\mathcal{H}_x/\mathcal{H}_K|$, confer with Eq. (4), we note that

$$\mathcal{H}^K_\omega \le 2\omega/n, \qquad \mathcal{H}^K_{3b} \le 2(\omega/n)^2(2-\alpha/a)^2$$

$$\mathcal{H}^K_{J_2} \le 2J_2\,(a/\alpha) \quad (20)$$

and we check the numeric values for the case of an orbiter around Europa whose semimajor axis is between 1600 and 2300 km. Using accepted values of Europa,[6]

$$\omega = 2.0\times 10^{-5}\,\mathrm{s}^{-1}, \qquad \mu = 3201\,\mathrm{km}^3\,\mathrm{s}^{-2}$$

$$\alpha = 1565\,\mathrm{km}, \qquad J_2\alpha^2 = 1051.315\,\mathrm{km}^2 \quad (21)$$

we obtain

$$\mathcal{H}^K_\omega < 0.08, \qquad \mathcal{H}^K_{3b} < 0.0053 \sim 0.08^2$$

$$\mathcal{H}^K_{J_2} < 0.0013 \sim 0.08^3$$

Note that the J_2 effect is of higher order than the third-body perturbation for an orbiter around Europa. Therefore, considering the upper bound of $\mathcal{H}^K_\omega$ as the small parameter ϵ, we write Eq. (3) as

$$\mathcal{H} = \sum_{i=0}^{3}\left(\frac{\epsilon^i}{i!}\right)\mathcal{H}_i \quad (22)$$

where $\mathcal{H}_0 = \mathcal{H}_K$ and

$$\mathcal{H}_1 = -\tilde{\omega} H$$

$$\mathcal{H}_2 = \tilde{\omega}^2 r^2 [1 - 3(\cos h \cos u - \cos i \sin h \sin u)^2]$$

$$\mathcal{H}_3 = J_2'(\mu/r)(\alpha/r)^2 P_2(\sin i \sin u)$$

with $J_2' = (6/\epsilon^3) J_2$. If we apply perturbation theory to order $\mathcal{O}(\epsilon^3)$, we arrive exactly at the third-order Lidov–Kozai model, Eq. (14). Of course, the generating function of the transformation will be different from the preceding case. Thus, to $\mathcal{O}(\epsilon^3)$, the third-order Lidov–Kozai model applies to Europa, but this model also applies to other dynamic systems provided they accept any of the two proposed sortings of the Hamiltonian terms.

Twice-Reduced Hamiltonian System on S^2

Once the Dealunay normalization removes the mean anomaly, for each value of the integral L, the motion is obtained from Eq. (8) by solving the differential system

$$\dot{g} = \frac{\partial \mathcal{H}'}{\partial G}, \qquad \dot{h} = \frac{\partial \mathcal{H}'}{\partial H}, \qquad \dot{G} = -\frac{\partial \mathcal{H}'}{\partial g}, \qquad \dot{H} = -\frac{\partial \mathcal{H}'}{\partial h} \quad (23)$$

and the quadrature

$$l = \int \left(\frac{\partial \mathcal{H}'}{\partial L} \right) \mathrm{d}t$$

That is, each point of the reduced system (23) corresponds to a different ellipse with a fixed semimajor axis. This orbit space is characterized by the angular momentum $\boldsymbol{G} = \boldsymbol{x} \times \boldsymbol{X}$ and the Laplace vector $\boldsymbol{A} = (L/\mu)[\boldsymbol{X} \times \boldsymbol{G} - (\mu/r)\boldsymbol{x}]$ because they do not depend on the mean anomaly. Alternatively, Moser orbital elements

$$\boldsymbol{f} = \boldsymbol{A} + \boldsymbol{G}, \qquad \boldsymbol{g} = \boldsymbol{A} - \boldsymbol{G} \quad (24)$$

are used to represent the motion of the reduced system (23). (See Ref. 21, for instance.) These elements have the same magnitude $\boldsymbol{g} \cdot \boldsymbol{g} = \boldsymbol{f} \cdot \boldsymbol{f} = L^2$ and can be identified with two points on a sphere of radius L. That is, the phase space of the reduced system (23) has the topological structure $S^2 \times S^2$.

The second Lie transform removes the argument of the node, and the third component of the angular momentum becomes an integral. The double-reduced Hamiltonian Eq. (11) corresponds to a one-DOF system related to the dynamics of the eccentricity and argument of perigee. However, the (g, G) representation corresponds to a cylindrical map of the reduced space, where the dynamics around circular orbits is complex because circular orbits are not represented by a point, but by the border of the cylinder $G = L$. This virtual singularity is introduced by the cylindrical representation. As demonstrated in Ref. 22, the double-reduced space of perturbed Keplerian systems is diffeomorphic to a sphere S^2, not a cylinder, whose radius is a function of each pair of values (L_0, H_0).

It is on the sphere where we fully analyze the influence of each parameter on the stability and bifurcations of frozen orbits. Using the Coffey et al.[23] variables,

$$\xi_1 = G\,L\,e \sin i \cos g, \qquad \xi_2 = G\,L\,e \sin i \sin g$$

$$\xi_3 = G^2 - \tfrac{1}{2}(L^2 + H^2) \quad (25)$$

we immediately check that the radius of the sphere is

$$R = \sqrt{\xi_1^2 + \xi_2^2 + \xi_3^2} = \tfrac{1}{2}(L^2 - H^2) \quad (26)$$

For a fixed pair of values of the integrals (L_0, H_0), each point in the sphere $S^2_{L_0, H_0}$ corresponds to a family of ellipses differing in the argument of the node. An arbitrary point on the sphere $(\xi_1^0, \xi_2^0, \xi_3^0)$ corresponds to a family of ellipses with eccentricity and argument of perigee given by

$$e = \left(R - \xi_3^0\right)^{\frac{1}{2}} \Big/ L, \qquad \tan g = \xi_2^0 \Big/ \xi_1^0$$

The "north pole" of the sphere $(G = L)$ corresponds to a family of circular orbits with inclination $\cos i = H_0/L_0$. The "south pole" $(G = H)$ represents the family of equatorial elliptic orbits with eccentricity $e = \sqrt{1 - H_0^2/L_0^2}$, differing in the argument of the perigee.

Proceeding as Coffey et al.[9] did, first we write the Hamiltonian as $\mathcal{K} = \mathcal{K}(\xi_2, G)$. Then, the differential equations of the system on the sphere are obtained from Liouville equations, $\dot{\xi}_i = \{\xi_i, \mathcal{K}\}$,

$$\dot{\xi}_1 = 2G \left(\frac{\partial \mathcal{K}}{\partial \xi_2} \right) \xi_3 - \left(\frac{\partial \mathcal{K}}{\partial G} \right) \xi_2$$

$$\dot{\xi}_2 = \left(\frac{\partial \mathcal{K}}{\partial G} \right) \xi_1, \qquad \dot{\xi}_3 = -2G\,\xi_1 \left(\frac{\partial \mathcal{K}}{\partial \xi_2} \right) \quad (27)$$

Thus, Eq. (14) is transformed to

$$\mathcal{K} = \tfrac{1}{8}(\omega/\mu)^2 G^2 L^2 \big[2\beta\,(1 - 3H^2/G^2)/(G^5 L^5) + 6 - 3H^2/G^2 - 5L^2/G^2 + 15\xi_2^2 \big/ G^4 + \delta\left(24 + H^2/G^2 - 25L^2/G^2 + 15\xi_2^2 \big/ G^4\right) \big] \quad (28)$$

from which we obtain

$$\dot{\xi}_1 = \tfrac{3}{4}(\omega/\mu)^2 G L^2 \xi_2 \big\{ 6 + (1 - 5H^2/G^2)\beta/(G^5 L^5) + (1 + \delta)\big[5\xi_2^2 \big/ G^4 + 2 - 5(H^2 + L^2)/G^2 \big] \big\}$$

$$\dot{\xi}_2 = -\tfrac{3}{4}(\omega/\mu)^2 G L^2 \xi_1 \big[6 + (1 - 5H^2/G^2)\beta/(G^5 L^5) + (1 + \delta)\left(5\xi_2^2 \big/ G^4 - 8 \right) \big]$$

$$\dot{\xi}_3 = -(15/2)(\omega/\mu)^2 (L^2/G) \xi_1 \xi_2 (1 + \delta) \quad (29)$$

Relative Equilibria

Our next task is to identify the equilibria in terms of the parameters H and L (relative equilibria of the full system). The roots of the averaged system in the open domain $0 < |H| \le G \le L$ have been obtained using Delaunay variables from the equations $\dot{g} = 0$ and $\dot{G} = 0$. Here, we take the system on $S^2_{L,H}$ to guarantee that we search for all of the possible roots by equating Eqs. (29) to zero. The condition, $\dot{\xi}_3 = 0$, shows that the equilibria, if any, can occur only for ξ_1 and/or $\xi_2 = 0$.

We will identify all of the roots from an algebraic point of view. Then, according to the dynamic constraints $|H| \le G \le L$ and $0 \ll G$, and also the constrains imposed on the values of L by the model, more restricted conditions are taken.

Roots at Poles of Sphere

From Eq. (29), we can see that the north and south poles $(\xi_1 = \xi_2 = 0)$ are always equilibrium points for any value of the parameters. They correspond to families of circular orbits and equatorial orbits, respectively.

Roots in Meridian $\xi_1 = 0$ (g = ±90 Degree)

When $\xi_1 = 0$, we obtain $\dot{\xi}_2 = \dot{\xi}_3 = 0$ in Eqs. (29). The last condition, $\dot{\xi}_1 = 0$, results in

$$3(1 - \delta) L^5 G^7 - 5(1 + \delta) H^2 L^7 G^3 + \beta G^2 - 5\beta H^2 = 0 \quad (30)$$

The equilibria correspond to the roots of polynomial (30), of degree 7 in G, that fulfill the condition $|H| \le G \le L$.

Roots in Meridian $\xi_2 = 0$ (g = 0 and 180 Degree)

From the second equation of Eq. (29), again we obtain a polynomial of degree 7 in G,

$$2(1 + 4\delta)\, L^5 G^7 - \beta G^2 + 5\beta H^2 = 0 \quad (31)$$

Again, the equilibria are the roots of Eq. (31) that satisfy $|H| \le G \le L$.

Bifurcations Lines and Regions in Parameter Plane (L, H)

Identification of regions on the space of parameters for which there are a different number of roots implies a different qualitative dynamic behavior. In carrying out this search, it is important to look for possible multiple roots of the equations. The conditions that must satisfy the parameters to obtain these multiple roots are the bifurcation lines. In this paper we take fixed values for the physical parameters: those corresponding to Europa. Then, we find bifurcation lines in the (L, H) plane. These lines define several regions in the parameter plane. Because of the information provided by bifurcation lines (appearance and disappearance of roots when crossing them), we identify the number of roots in each region.

In the search for bifurcation lines we proceed as did Lidov and Yarskaya.[5] Basically, the bifurcation lines are of two types. The first type is related to pitchfork bifurcations of families of orbits represented at the north and south poles of the sphere, which are always roots of our system for any value of the parameters. We find conditions on H and L for these bifurcations imposing on Eqs. (30) and (31) that they take the values $G = L$ or $G = H$. The second type, saddle-center bifurcations, are related to elliptic orbits at specific inclinations. In this case, we find these bifurcation imposing conditions for multiple roots.

Bifurcations in Meridian $\xi_1 = 0$

Imposing the limit values for G in Eq. (30), we identify two bifurcation lines related to bifurcations of the poles. Thus, bifurcations of the north pole ($G = L$) occur along the line

$$n \equiv 3(1-\delta)L^{12} - 5(1+\delta)H^2L^{10} + \beta L^2 - 5\beta H^2 = 0 \quad (32)$$

(n for north), whereas bifurcations of the south pole ($G = |H|$) occur along the line (s for south)

$$s \equiv 3(1-\delta)L^5|H^5| - 5(1+\delta)L^7|H^3| - 4\beta = 0 \quad (33)$$

Bifurcations in Meridian $\xi_2 = 0$

The limits on Eq. (31) give us bifurcations of the north pole ($G = L$) along the line n_0 (subindex 0 for $g = 0$ and 180 deg),

$$2(1+4\delta)L^{12} - \beta L^2 + 5\beta H^2 = 0 \quad (34)$$

and bifurcations of the south pole ($G = |H|$) along the line s_0

$$(1+4\delta)L^5|H|^5 + 2\beta = 0 \quad (35)$$

Other Bifurcations

We also find double roots that are not bifurcations of the poles along the meridian $g = 0$ and 180 deg. They occur for the values of L and H that satisfy the implicit relation

$$\beta^2 - 7^7 H^{10} L^{10}[1 + 8\delta(1+2\delta)] = 0 \quad (36)$$

obtained by equating Eq. (31) to its partial derivative with respect to G. Equation (36) defines the bifurcation line m. However, it only exists for double roots $G(H, L)$ that satisfy the dynamic constraint $H \le G \le L$. As we will see later, this double root corresponds to a saddle-node bifurcation at $\xi_2 = 0$.

Parameter Plane

Lidov and Yarskaya[5] made a systematic study of the bifurcation lines on the cylinder reduced space over the parameter plane ($\sigma = H/L$, $\gamma = \beta/L^{10}$). We make a similar analysis on the sphere by adding higher order terms.

Note that we must fix the values of the parameters β and (ω/μ^2). Because the main motivation of this work is the study of the dynamic behavior around Europa, we used the values given in Eq. (21) that produce

$$\beta = 2.8274 \times 10^{33}\,\mathrm{km}^{20}/\mathrm{s}^{10}$$

$$(\omega/\mu^2) = 1.9519 \times 10^{-12}\,\mathrm{s}^3/\mathrm{km}^6$$

Figure 1 presents the bifurcation lines and regions in the parametric plane (L, H). The numbers inside each region correspond to the total number of equilibria (or frozen orbits). The two vertical dashed lines bound the range of validity for an orbiter around Europa. The lower bound $L = 2300\,\mathrm{km}^2/\mathrm{s}$ corresponds to a semimajor axis equal to the equatorial radius of Europa, and the upper bound is estimated as follows. The commensurability of the third-body and J_2 perturbations imply applying $(\mathcal{H}^K_{3b})^2 \ll \mathcal{H}^K_{J_2}$ to Eq. (20). We solve this inequality for the semimajor axes, obtaining $a \ll 4200$ km, less than one-third of the Hill radius $r_H \approx 13{,}600$ km. The conservative limit $L = 3000\,\mathrm{km}^2/\mathrm{s}$ ($a \approx 2800$ km) for the upper bound corresponds to two-thirds of the maximim value $a = 4200$ km.

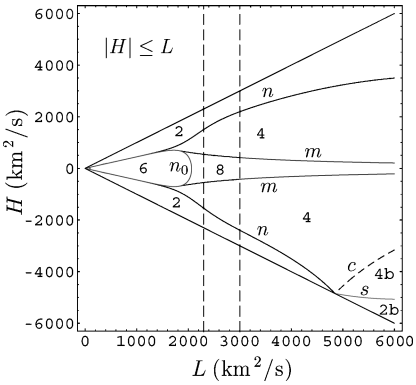

Fig. 1 Bifurcation lines and regions in parameter plane.

Finally, note that, following the Descartes rule, the maximum number of positive roots of Eqs. (32–36) is affected only by changes in sign of the coefficients. Therefore, no fundamental changes are expected for different values of $\beta > 0$. The case $\beta < 0$ of prolate bodies is completely different and deserves a separate study.

Stability by Painting Flow

The flow can be represented by contour plots of the Hamiltonian equation (14) that correspond to the orbits of the double-reduced system. Alternatively, the values of the Hamiltonian equation (28) can be used to assign colors to points (ξ_1, ξ_2, ξ_3) on the sphere. Then, each orbit is represented by a succession of contiguous points of the same color. This technique is known as painting phase spaces,[8,9] and is very useful for exposing the flow around the equilibria. The only limitation is that we do not know the sense of the motion at each colored trajectory. However, the evaluation of $\dot{g}$ in Eq. (16) for just a few points will provide that sense. Finally, note that color diagrams do not provide quantitative information because the color coding is designed to enhance contrast, and the same color could be assigned to different values of the Hamiltonian.

After finding the equilibria and their bifurcations in the (L, H) plane as functions of the parameters, we investigate the stability character of each equilibrium and discuss in detail the different regions delimited by the bifurcation lines in Fig. 1. To understand the flow, Fig. 2 presents orthographic north and south poles views of the sphere in different regions of the parameter plane. In each case, the values (L, H) are specified at the bottom of the corresponding sphere, whereas the number of equilibria are at the top.

The analysis starts from the circular equatorial orbits that correspond to $L = |H|$, the inclined straight lines of Fig. 1 that bound the parameter plane. We refer to each region of Fig. 1 by the number of equilibria with an index, when necessary, which is the sign of H inside that region (positive for direct inclination orbits and negative for retrograde inclination orbits).

Region 2^+

This region is bounded by the lines n and $L = H$. Inside this region, both poles are always stable equilibria. That is, we find stable circular inclined and elliptic equatorial orbits. Figure 2 shows this with image 2, where the poles are elliptic fixed points and the perigee of the elliptic inclined orbits rotates around the poles. For decreasing values of H, the circular orbits become more and more inclined, until the line n is found where a pitchfork bifurcation of the north pole occurs. The circular orbits become unstable, and two eccentric orbits bifurcate with their perigee frozen at 90 and 270 deg,

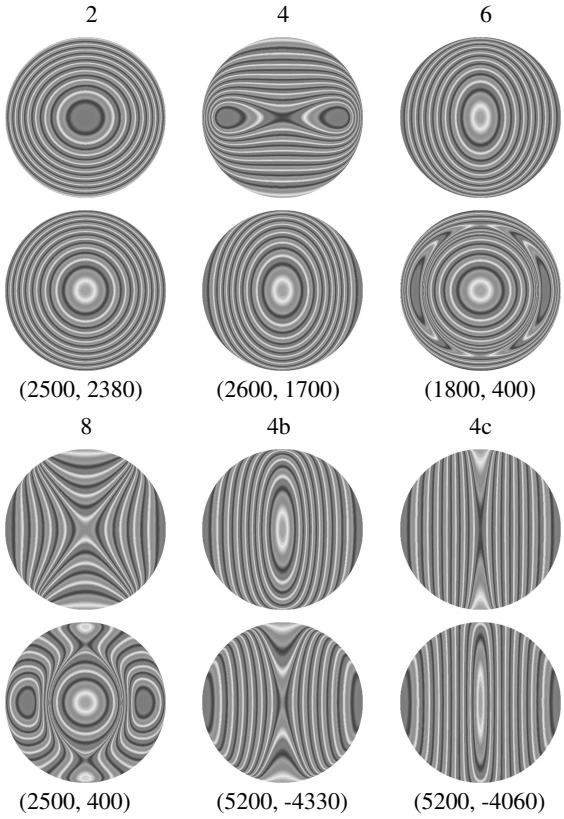

Fig. 2 Phase portraits for different (L, H): abscissas, ξ_2 and ordinates, ξ_1.

respectively. The inclination where this bifurcation occurs depends on the semimajor axis. For a given value of a (or L) inclination is obtained by solving Eq. (32) with $H = L\cos i$. Thus, for example, the stability of an orbiter in a circular orbit with an averaged semimajor axis $a = 2000$ km ($L \approx 2530$) changes at $i = 45.29$ deg.

Region 4^+

This region is bounded by the lines n and n_0, which join at the origin, and the line m that is tangent to n_0 at $L \approx 1819$ ($a \approx 1034$ km). The north pole is unstable, the south pole is stable, and there are two stable equilibria corresponding to two orbits with their perigee frozen at 90 and 270 deg, respectively. As illustrated with image 4 in Fig. 2, orbits close to the stable equilibria show oscillation of the perigee around the frozen value. In any other case the perigee rotates. For decreasing values of H the eccentricity of the frozen orbits notably increases. Thus, for instance, for an orbiter with an averaged semimajor axis $a = 2000$ km ($L \approx 2530$) we solve Eq. (30) for G. For $H = 1750$, close to n, we obtain a frozen orbit with eccentricity $e = 0.13$ and inclination $i = 45.78$ deg. For $H = 1500$, $e = 0.39$, and $i = 49.87$ deg. For $H = 1000$, $e = 0.66$, and $i = 58.14$ deg.

For orbits close to the origin (L small) this region is bounded by the line n_0, where a new bifurcation of the north pole occurs. Circular orbits become stable, and two new unstable eccentric orbits bifurcate with their perigees at 0 and 180 deg and with inclinations close to the critical inclination value of 63.4 deg. The other bound of this region is the line m, where a saddle-node bifurcation occurs at the meridians $g = 90$ and 270 deg. The stability of the poles does not change at m.

Region 6

This region is bounded by the line n_0 and the origin (image 6, Fig. 2). Here, the north and south poles are stable equilibria. There are two unstable equilibria corresponding to elliptic orbits with perigee at 0 and 180 deg and two stable equilibria corresponding to frozen elliptic orbits with perigees at $g = 90$ and 270 deg. Inside this region, the influence of the oblateness clearly predominates over the third-body perturbation. This behavior, analogous to that of the "main problem" of the artificial satellite,[23] is not of interest for an orbiter around Europa because orbits in this region have smaller semimajor axes than Europa's equatorial radius.

At the border of regions 6 and 8 we find that n_0 produces global changes in the dynamics. The stable equilibria of the meridian $\xi_2 = 0$ collapse to the north pole, which becomes unstable, and a saddle-node bifurcation occurs with two stable and two unstable equilibria at $\xi_2 = 0$.

Region 8

Region 8 is bounded by the line n_0 and both lines m, encompassing direct ($H > 0$) and retrograde ($H < 0$) inclination orbits. Inside this region we find eight equilibria: the unstable north pole, the stable south pole, two unstable equilibria at $\xi_2 = 0$ ($g = 0$ and 180 deg), and four stable equilibria corresponding to frozen orbits with perigees at 0, 90, 180, and 270 deg. Image 8 in Fig. 2 illustrates this behavior.

All of the frozen orbits are highly eccentric. For instance, for $a = 2000$ km ($L \approx 2530$) and $H = 490$, close to the upper line m, we solve Eqs. (30) and (31) for G. From the first we obtain two frozen orbits with $e = 0.89$, $i = 64.93$ deg, and $g = 90$ and 270 deg. From the second, two frozen orbits with $e = 0.84$, $i = 68.90$ deg, and $g = 0$ and 180 deg are obtained. All of these orbits impact the surface of Europa.

Region 4^-

Region 4^- is bounded by the lines n, n_0, m, and c. The behavior of the retrograde inclination orbits in this region is completely analogous to that of direct inclination orbits in region 4^+. Therefore, image 4 in Fig. 2 illustrates the flow inside this region. The image 4c at the bottom of the Fig. 2 shows the flow close to the bifurcation line c.

Region 4b

Region 4b is bounded by the lines c and s. The flow in this region is illustrated in image 4b in Fig. 2. There are four equilibria: the stable north pole, the unstable south pole, and two stable equilibria at the meridian $\xi_1 = 0$ ($g = 90$ and 270 deg). Despite that the number of roots does not change between regions 4^- and 4b, line c produces dramatic changes in the perigee dynamics of retrograde inclination orbits. Whereas in region 4b the south pole is unstable and the flow rotates around the stable north pole, we find the opposite behavior in region 4^-: unstable north pole and rotation around the stable south pole.

In fact, c is not a line, but an extremely narrow region bounded by two branches of different lines that almost superpose each other. Going from region 4b to region 4^-, we first find the line s_0, where a pitchfork bifurcation of the south pole occurs. The south pole becomes stable and two new unstable equilibria appear at $g = 0$ and 180 deg. Image 6 in Fig. 2 illustrates the flow in this small region, despite its correspondence to region 6. These unstable equilibria move very fast toward the north pole and immediately collapse in a pitchfork bifurcation of the north pole at a new branch of n_0.

Region 2^-

Region 2^- is bounded by the lines n and $L = -H$. The behavior of the retrograde inclination orbits in this region is completely analogous to that of direct inclination orbits in region 2^+. Therefore, image 2 in Fig. 2 illustrates the flow on this region. Note, however, that region 2^- only exists for $a \leq 7342.24$ km ($L \leq 4847.94$), whereas region 2^+ exists for any semimajor axis.

Region 2b

Region 2b is bounded by the lines s and $L = -H$. In this region, $a \geq 7342.24$ km, and we only find rotation of the perigee of the retrograde inclination orbits around the poles, which are stable. The stability of the equatorial orbits changes to instability at the line s, where a pitchfork bifurcation of the south pole occurs with two stable equilibria at the meridian $\xi_1 = 0$ ($g = 90$ and 270 deg).

Returning to Original System

In spite of the dynamic richness of our model, the region that applies to Europa is relatively simple. As shown in Fig. 1, we only find the pitchfork bifurcation of the north pole in the meridian $g = \pm 90$ deg, produced when crossing the lines n, and the saddle-node bifurcation of elliptic orbits produced in the meridian $g = 0$ and 180 deg when crossing the lines m. If our analytical theory represents the real problem, we should find similar behavior in the original system.

For our comparisons, we use Ref. 10, where numerical continuation of periodic orbits was used to determine stability regions for an orbiter around Europa.

Our first comparison is related to the change in the stability of almost-circular orbits. A variety of families of almost-circular periodic solutions of the nonaveraged system Eq. (1) was computed in Ref. 10 for different repetition cycles. Reference 10 showed that the stability character of the almost-circular periodic orbits (in the rotating frame) changes at certain critical inclinations where eccentric stable solutions bifurcate. We use the collection of critical orbits computed there and compare them with the bifurcation line n. For circular orbits, $G = L$ and $H = L\cos i$. Therefore, we write Eq. (32) as

$$6 + 4\beta/L^{10} = \left[1 + (\beta/L^{10}) + \tfrac{9}{8}(\omega/\mu^2)L^3\cos i\right](3 + 5\cos^2 i) \quad (37)$$

and plot the line n in terms of semimajor axis and inclination. Figure 3 shows the perfect agreement between analytical (full line) and numerical results (dots).

Each point on the sphere corresponds to a family of orbits. Furthermore, each equilibrium of the reduced system corresponds to a family of frozen orbits with different arguments of the node. Therefore, initial conditions obtained from equilibria of the reduced phase space should correspond to a frozen orbit of the original, nonaveraged problem. This behavior can be easily checked. For instance, introducing the values $L = 2650$ and $H = 1000$ in Eq. (30), we obtain $G = 1951.36$ for the equilibria in the meridian $g = \pm 90$ deg. From these values, without the need of undoing the canonical transformations, we obtain the orbital elements $a = 2193.85$ km, $e = 0.69$, and $i = 58.53$ deg. A long-term propagation of these elements shows small oscillations of the argument of the perigee $85 < g < 95$ deg and of the eccentricity $0.66 < e < 0.74$. Figure 4 shows the evolution of e and g during a 1-year propagation. Furthermore, slight modifications of the corresponding initial conditions easily lead to an exact periodic orbit in the rotating frame after a 25-repetition cycle, with averaged orbital elements $a = 2177.17$ km, $e = 0.747$, $i = 60.86$ deg, and $g = 270$ deg. That solution is presented in Fig. 5.

With respect to the saddle-node, we introduce the values $L = 2650$ and $H = 300$ in Eq. (31), obtaining $G = 675.3$ for the unstable equilibrium and $G = 1537.8$ for the stable equilibrium at the meridian

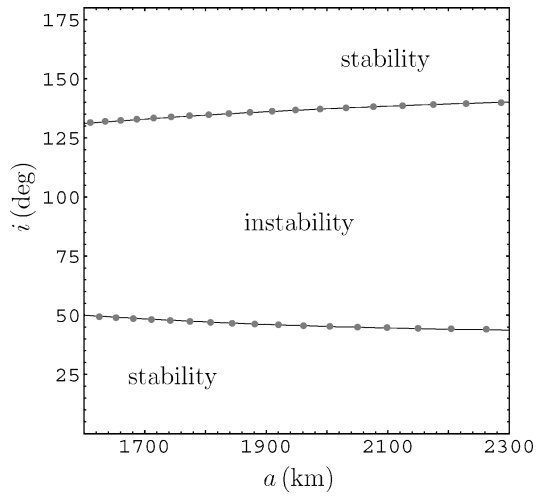

Fig. 3 Change in stability of almost circular orbits: ——, analytic vs . . . , numeric.

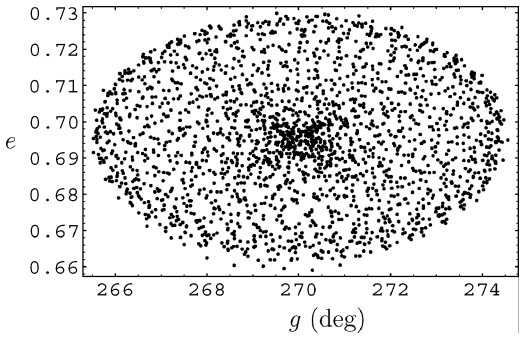

Fig. 4 Frozen orbit, $a = 2193.85$ km and $i = 58.53$ deg, 1-year propagation.

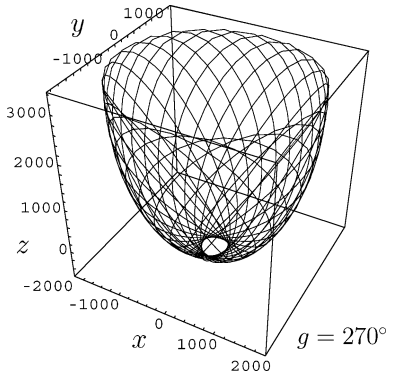

Fig. 5 Periodic orbit in kilometers after 25 cycles.

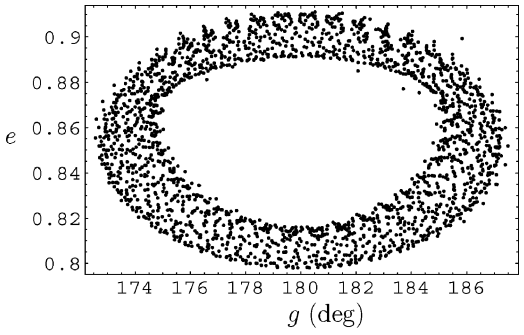

Fig. 6 Frozen orbit, $a = 2193.85$ km and $i = 78.75$ deg, 1-year propagation.

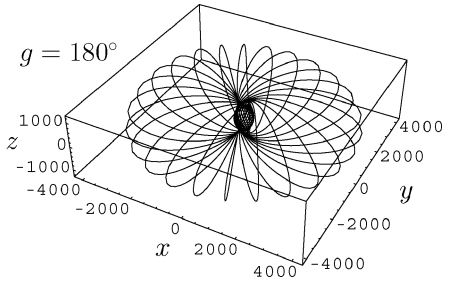

Fig. 7 Periodic orbit in kilometers after 25 cycles.

$g = 0$ and 180 deg. A long-term propagation of the stable equilibrium ($a = 2193.85$ km, $e = 0.81$, and $i = 78.75$ deg) shows that it corresponds to a frozen orbit whose argument of the perigee oscillates between 172 and 188 deg, and whose eccentricity oscillates in the range $0.798 < e < 0.915$ (Fig. 6). Again, we improved these initial conditions to obtain a true periodic orbit in the rotating frame after a 25-repetition cycle, with averaged orbital elements $a = 2253.39$ km, $e = 0.84$, $i = 76.53$ deg, and $g = 180$ deg. Figure 7 presents the results.

Both preceding examples correspond to high-ellipticity orbits that, of course, impact on the surface of Europa. We provide

them here to show the agreement between analytical and numerical results.

Conclusions

A third-order analytical theory for the Lidov–Kozai model incorporates several relevant features of the dynamics around planetary satellites, notably the nonsymmetry of retrograde and direct inclination orbits and the existence of stable elliptic orbits that do not bifurcate from almost-circular orbits. After the mean anomaly and the argument of the node have been removed by Lie transforms, classical polynomial algebra provides the complete description of families of frozen orbits and their bifurcations.

The application of this model to Europa shows full agreement with previous numerical results. The model is not restricted to Europa and applies to other dynamic systems, provided that they accept the sorting of the Hamiltonian terms proposed in this paper.

The results of this paper are directly applicable to the orbital motion of the proposed Jupiter Icy Moons Orbiter mission to the Galilean moons. However, the validity of our theory for practical purposes is limited to a region close enough to the central body, where Hill's equations are suitable for modeling the planetary perturbation. Generating accurate ephemeris still requires a higher-order theory. This work is in progress, and we expect to report a fourth-order analytical theory in the near future.

Acknowledgments

We acknowledge support of the Spanish Ministry of Technology and Science (Projects ESP2002-02329, BFM2002-03157, BFM2003-02137, and ESP2004-04376) and of Fundación Séneca of Región de Murcia. Discussions with V. Lanchares of the University of La Rioja were very helpful in the development of this work. Thanks are due to A. Abad of the University of Zaragoza for his software for painting Hamiltonians.

References

[1]"Jupiter Icy Moons Orbiter," Jet Propulsion Lab., California Inst. of Technology, Pasadena, CA, URL: http://www.jpl.nasa.gov/jimo [cited 31 Dec. 2004].

[2]Hill, G. W., "Researches in Lunar Theory," *American Journal of Mathematics*, Vol. 1, No. 1, 1878, pp. 129–147.

[3]Kozai, Y., "Motion of a Lunar Orbiter," *Publications of the Astronomical Society of Japan*, Vol. 15, No. 3, 1963, pp. 301–312.

[4]Lidov, M. L., "On the Approximated Analysis of the Orbit Evolution of Artificial Satellites," *Dynamics of Satellites*, edited by M. Roy, Springer-Verlag, Berlin, 1963, pp. 168–179.

[5]Lidov, M. L., and Yarskaya, M. V., "Integrable Cases in the Problem of the Evolution of a Satellite Orbit Under the Joint Effect of an Outside Body and of the Noncentrality of the Planetary Field," *Kosmicheskie Issledovaniya*, Vol. 12, March–April 1974, pp. 155–170; *Cosmic Research*, Vol. 12, No. 2, 1974, pp. 139–152 (translation).

[6]Scheeres, D. J., Guman, M. D., and Villac, B. F., "Stability Analysis of Planetary Satellite Orbiters: Application to the Europa Orbiter," *Journal of Guidance, Control, and Dynamics*, Vol. 24, No. 4, 2001, pp. 778–787.

[7]Deprit, A., "Delaunay Normalizations," *Celestial Mechanics*, Vol. 26, No. 1, 1982, pp. 9–21.

[8]Coffey, S. L., Deprit, A., Deprit, E., and Healy, L., "Painting the Phase Space Portrait of an Integrable Dynamical System," *Science*, Vol. 247, No. 4944, 1990, pp. 833–836.

[9]Coffey, S. L., Deprit, A., and Deprit, E., "Painting Phase Spaces to Put Frozen Orbits in Context," American Astronautical Society, Paper 91-427, Aug. 1991.

[10]Lara, M., and San-Juan, J. F., "Phase Space Structure for Three-Dimensional Motion around Europa," American Astronautical Society, Paper 03-233, Jan. 2003.

[11]Markellos, V. V., Roy, A. E., Perdios, E. A., and Douskos, C. N., "A Hill Problem with Oblate Primaries and the Effect of Oblateness on Hill Stability of Orbits," *Astrophysics and Space Science,* Vol. 278, No. 3, 2001, pp. 295–304.

[12]Papadakis, K. E., "The Planar Hill Problem with Oblate Primaries," *Astrophysics and Space Science*, Vol. 293, No. 3, 2004, pp. 271–287.

[13]Serrano, S., Abad, A., and San-Juan, J. F., "Ordenación Asintótica del Potencial Terrestre," *Monografías de la Academia de Ciencias de la Universidad de Zaragoza*, Vol. 22, March 2003, pp. 103–112.

[14]Serrano, S., "Teorías Analíticas del Movimiento de un Satélite Artificial Alrededor de un Planeta. Ordenación Asintótica del Potencial en el Espacio Fásico," Ph.D. Dissertation, Departamento de Matemática Aplicada, Univ. de Zaragoza, Zaragoza, Spain, June 2003; also *Monografías del Seminario García de Galdeano*, Vol. 28, 2003.

[15]Deprit, A., "Canonical Transformations Depending on a Small Parameter," *Celestial Mechanics*, Vol. 1, No. 1, 1969 pp. 12–30.

[16]Deprit, A., and Coffey, S. L., "Third-Order Solution to the Main Problem in Satellite Theory," *Journal of Guidance, Control, and Dynamics*, Vol. 5, No. 4, 1982 pp. 363–371.

[17]Osácar, C., "Estudio del Movimiento de Sistemas Estelares," Ph.D. Dissertation, Departamento de Físiča Téorìca, Servicio de Publicaciones, Univ. de Zaragoza, Zaragoza, Spain, Jan. 1990.

[18]Palacián, J., "An Analytical Solution for Artificial Satellites at Low Altitudes," *Proceedings of the Conference on Dynamics and Astrometry of Natural and Artificial Celestial Bodies*, edited by K. Kurzyńska, F. Barlier, P. K. Seidelmann, and I. Wytrzyszczak, Astronomical Observatory of A. Mickiewicz, Univ. of Poznań, Poznań, Poland, 1994, pp. 365–370.

[19]Palacián, J., San Juan, J. F., and Yanguas, P., "Analytical Theory for the Spot Satellite," American Astronautical Society, Paper 97-125, Feb. 1997.

[20]Serrano, S., and San Juan, J. F., "ATESAT: Revisited and Improvements. Analytical Theory and Numerical Validation for a SPOT-like Satellite," Centre National d'Etudes Spatiales, Rept. DTS/MPI/MS/MN/2000-013, Toulouse, France, Dec. 2000.

[21]Tabor, J. L., and Vedder, J. D., "Long-Term Evolution of Uncontrolled Geosynchronous Orbits: Orbital Debris Implications," *Journal of the Astronautical Sciences*, Vol. 40, No. 3, 1992, pp. 407–418.

[22]Cushman, R., "Reduction, Brouwer's Hamiltonian and the Critical Inclination," *Celestial Mechanics* Vol. 31, Dec. 1983, pp. 409–429; also Errata, Vol. 33, Aug. 1984, p. 297.

[23]Coffey, S., Deprit, A., and Miller, B., "The Critical Inclination in Artificial Satellite Theory," *Celestial Mechanics*, Vol. 39, No. 4, 1986, pp. 365–406.